

Article

Temperature Modeling of AZ31B Alloy Plate during Open-Roller Conveying Process Considering Air-Cooling Characteristics

Shuang Xu ¹, Zebin Wang ¹, Weitao Jia ^{2,*} , Xingrui Chen ^{3,*}  and Yunyun Dong ⁴¹ College of Data Science, Taiyuan University of Technology, Taiyuan 030024, China² College of Mechanical Engineering, Taiyuan University of Science and Technology, Taiyuan 030024, China³ Queensland Centre for Advanced Materials Processing and Manufacturing (AMPAM), School of Mechanical and Mining Engineering, The University of Queensland, Brisbane, QLD 4072, Australia⁴ College of Software, Taiyuan University of Technology, Taiyuan 030024, China

* Correspondence: jwtxs1314@tyust.edu.cn (W.J.); xingrui.chen@uq.edu.au (X.C.)

Abstract: In the process of open-roller conveying, magnesium alloy plates easily produce temperature drops and uneven temperatures. Ignoring the heat dissipation caused by the contact between the plate and the roller table, the process can be described as a process of air cooling. The present study aimed to investigate the temperature distribution and evolution of a magnesium alloy plate during the process. The air-cooling process of the AZ31B magnesium alloy plate was investigated and analyzed in detail under different initial temperatures and plate thicknesses, with a specific focus on the temperature distribution along both the width and thickness directions. The results show that the temperature-difference curves between the end face and the center under different air-cooling conditions appeared to have four stages: rapid increase, slow increase, basic stable and slow decline. To facilitate the establishment of the temperature model, the whole air-cooling process was approximately divided into two independent one-dimensional heat-conduction processes in the thickness direction and the width direction. Subsequently, one-dimensional steady-state heat-conduction models were developed in various directions, based on the fundamental principles of heat transfer and assuming that the adjacent temperature-drop layer satisfied the quadratic function distribution. Through the superposition of cooling with time in two directions, the temperature evolution at different positions in the process of air cooling can be solved accurately.

Keywords: open-roller conveying; air cooling; AZ31B magnesium alloy; temperature model; heat transfer



Citation: Xu, S.; Wang, Z.; Jia, W.; Chen, X.; Dong, Y. Temperature Modeling of AZ31B Alloy Plate during Open-Roller Conveying Process Considering Air-Cooling Characteristics. *Crystals* **2023**, *13*, 407. <https://doi.org/10.3390/cryst13030407>

Academic Editor: Shouxun Ji

Received: 14 February 2023

Revised: 24 February 2023

Accepted: 26 February 2023

Published: 27 February 2023



Copyright: © 2023 by the authors. Licensee MDPI, Basel, Switzerland. This article is an open access article distributed under the terms and conditions of the Creative Commons Attribution (CC BY) license (<https://creativecommons.org/licenses/by/4.0/>).

1. Introduction

Roller conveying is a necessary step to complete the rolling industrial production of metal plates. Currently, open rollers or closed rollers are widely used to transport metal plates in production lines. Magnesium alloy has the characteristics of lower heat capacity and lower thermal conductivity, which lead to the following two phenomena: (1) In the process of roller conveying without auxiliary heat, temperature changes are very easily created because the heat dissipation and temperature differences are produced in the width and thickness directions of magnesium alloy plates. (2) Lower thermal conductivity can easily lead to the emergence of local temperature-drop zones, resulting in uneven temperatures in magnesium alloy plates. These two phenomena affect the formability and yield of plates during rolling deformation. To minimize the temperature drops in magnesium alloy plates during the roller conveying process and to ensure that the plates remain at the required temperature for subsequent rolling deformation, the roller conveying step needs to have the technical characteristics of continuity without interruption, fast speed, and closed auxiliary heat transmission. In this case, when using the traditional

methods involving contact-temperature measurement (such as using thermometer, point thermometer or other temperature measuring tools), it is difficult to track and detect the plate-temperature status in real time [1,2]. Therefore, the off-line prediction of plate temperature is particularly important.

During the open-roller conveying process, the heat transfer between the plate and its surrounding medium primarily involves heat conduction to the conveying roller, as well as convection and radiation with the surrounding air [3]. According to the Newton cooling formula, thermal conduction heat dissipation is proportional to the contact area [4]. Since the contact between the plate and the conveying roller is linear, the heat dissipation between them can be ignored [5]. According to one report [6], the heat-flux density per unit area of thermal radiation is proportional to the quartic difference between the absolute temperatures of the two radiation surfaces, and the heat-flux density per unit area of the thermal convection heat dissipation is proportional to the difference in temperature between the surrounding air and the plate. During the air-cooling process for conventional strip steel, there is a significant temperature difference between the strip and the surrounding air. As a result, convective heat transfer only contributes a small proportion to the overall heat dissipation. J. Q. Sun [7] estimated the comprehensive heat-transfer coefficient during the air-cooling process of a steel plate by assuming the heat-transfer mode of the steel plate in the heat-retention panel to be based on radiation. The results worked well for the prediction of the temperature history. Thus, considering that the accurate measurement and calculation of convective heat dissipation are difficult, the effect of convective heat transfer on the temperature of the strip plate can be ignored when calculating the temperature drop caused by air cooling [8]. However, compared with steel and aluminum plate and strip, magnesium alloy plates bear lower preheating temperatures (250~450 °C [9]), resulting in smaller temperature differences between these plates and the air. In addition, the volume-specific heat of magnesium alloy is smaller, which makes the temperature of magnesium alloy more sensitive to heat change [10]. Therefore, the air-cooling behavior of magnesium alloy plates is more intricate than that of conventional strip steel. It is necessary to fully consider the use of thermal radiation and convection to accurately solve the thermal changes in magnesium alloy plates during transportation. Obviously, the traditional air-cooling model of strip steel cannot accurately describe the cooling behavior of magnesium alloy plates [11].

This study aims to build a temperature model for the AZ31B alloy plate air-cooling process, taking into account the comprehensive effects of thermal radiation and convection heat dissipation. The real-time heat-dissipation temperature drop of the plates was tested. The method of “discrete and dimension reduction solution, combination of temperature drop in two directions” was used to establish a three-dimensional temperature-distribution model for the magnesium alloy plate during non-auxiliary heat-roller transportation. Finally, the prediction accuracy of the model was verified by the real-time temperature-measurement data for the AZ31B magnesium alloy plate. The model can provide an important basis for temperature control and auxiliary heat implementation in the conveying process, which is of great significance for improving the forming quality of wide magnesium alloy plates.

2. Materials and Methods

The material used in the experiment was AZ31B (Mg-3.01Al-0.95Zn) alloy plate, which underwent a milling process to remove any defects and oxide layers on its surface. The plate samples used in the real-time air-cooling-temperature-measurement experiment had identical lengths (300 mm) and widths (200 mm), but different thicknesses (8 mm, 15 mm and 31 mm, respectively). Figure 1 is the schematic diagram of real-time temperature measurement during open-roller conveying process. In the thickness-center layer of the plate, the thermocouple wire numbers along the width direction were TC1, TC2 and TC3 respectively, while on the surface of the plate, the thermocouple wire numbers along the width direction were TC4, TC5 and TC6 respectively. The TC1 and TC4 were used to measure the temperature at the width center, TC2 and TC5 were used to measure

the temperature at the 1/4 width position and TC3 and TC6 were used to measure the temperature at the edge. The high-frequency (100 Hz) temperature recorder (HIOKI LR8400-21) was used to detect the temperature distribution and changes of different plate parts during the air-cooling process in real time. To achieve this, ω -type thermocouples were utilized; they were made through exposed butt welding, with a conductor diameter of 0.06 mm. These thermocouples had a quick response time of approximately 0.03 s and an outer diameter of 2 mm. The thermocouple of the central layer was deployed by drilling holes in the plate surface (the diameter of the hole was 1 mm). After inserting the thermocouple, we filled the hole with magnesium shavings to fix the thermocouple. The thermocouple on the surface of the plate was fixed by welding. The initial temperature of the plate was set at 250, 300, 350 and 400 °C, while the maximum deviation was no more than ± 6 °C.

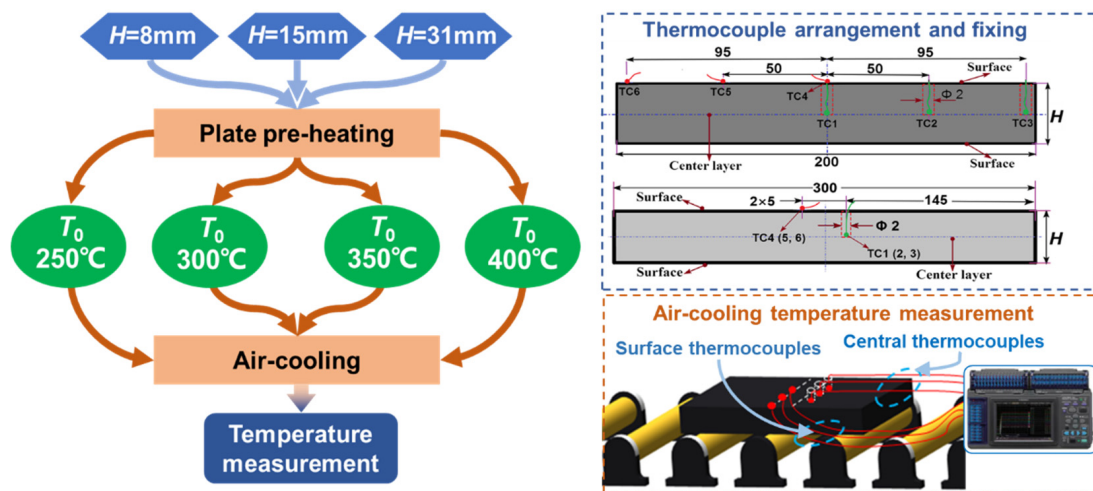


Figure 1. Real-time temperature measurement in air-cooling process.

3. Temperature Distribution and Evolution in Width and Thickness Directions

By calculating the temperature difference between the middle and the edge (ΔT_{width} , Equation (1)) and difference in temperature between the surface and middle layers of the thickness ($\Delta T_{thickness}$, Equation (2)), a quantitative evaluation was conducted on the distribution characteristics of temperature in terms of plate thickness and width during the air-cooling process. The larger the value, the greater the temperature difference and the higher the degree of temperature non-uniformity.

$$\Delta T_{width} = \frac{(T_{(TC1)} + T_{(TC4)}) - (T_{(TC3)} + T_{(TC6)})}{2} \quad (1)$$

$$\Delta T_{thickness} = \frac{(T_{(TC1)} + T_{(TC2)} + T_{(TC3)})}{3} - \frac{(T_{(TC4)} + T_{(TC5)} + T_{(TC6)})}{3} \quad (2)$$

Taking the air-cooling process of 15-mm- and 31-mm-thick slabs at initial temperatures of 250 °C and 400 °C as an example, Figures 2 and 3 show the variation in ΔT_{width} and $\Delta T_{thickness}$, respectively, over time. The B-splines (basic splines) were used for data-smoothing purposes. It can be seen from the figure that the change curves with time under the conditions of different plate thicknesses (15 mm, 31 mm) and different initial temperatures (250 °C, 400 °C) showed obvious unimodal characteristics, while the appearance of the peak value meant the generation of the maximum temperature gradient between temperature-measurement positions. The width-direction peak occurred at 150~200 s of air cooling, while that of the thick direction occurred at 140~185 s. The times of occurrence under the same conditions were approximately the same. For the pre-peak stage, the main heat-transfer mechanisms were the heat radiation and convection heat transfer from the slab to the air. In the width direction, because the edge had a greater air-contact area, the tem-

perature drop at the edge was greater than that at the middle, resulting in a sharp increase in the width-direction temperature difference, leading, in turn, to an enhancement in the slab's width-direction self-conduction. In the thickness direction, due to direct contact with the external environment, the temperature drop in the surface metal occurs first. As a result of the insulation between the internal metal and the external environment, the air-cooling effect was affected by the material's thermal resistance and was unable to swiftly penetrate into the interior, leading to the gradual expansion of the temperature-difference region, eventually extending to the central layer. Furthermore, the temperature gradient between the middle layer and the surface layer of the thickness gradually increased until the peak value was generated. During the post-peak stage, as the plate temperature decreased, the thermal radiation and convection effects gradually diminished. Simultaneously, owing to the full thermal conduction within the plate, the temperature difference in terms of heat dissipation between the middle and edge, as well as between the central and surface layers, gradually approached consistency. In the figure, it is shown that ΔT_{width} and $\Delta T_{thickness}$ decreased slowly.

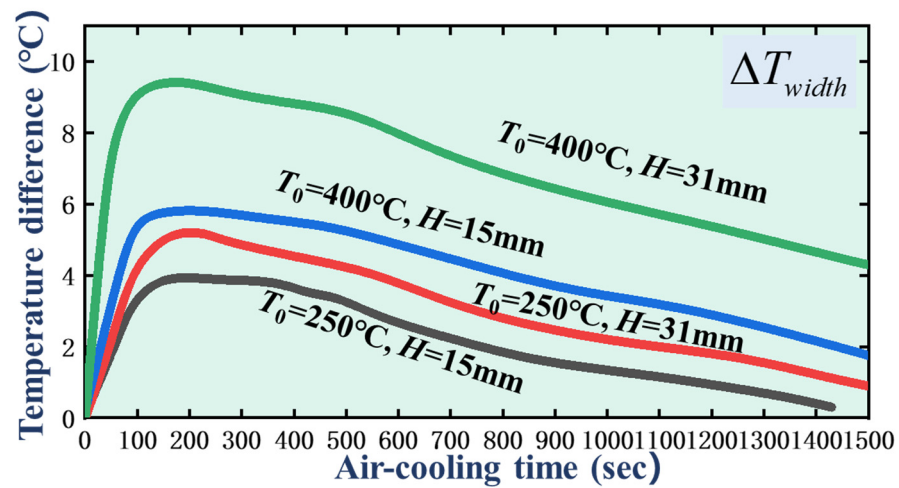


Figure 2. Variation in ΔT_{width} over time for plate with different thicknesses under 250 °C and 400 °C.

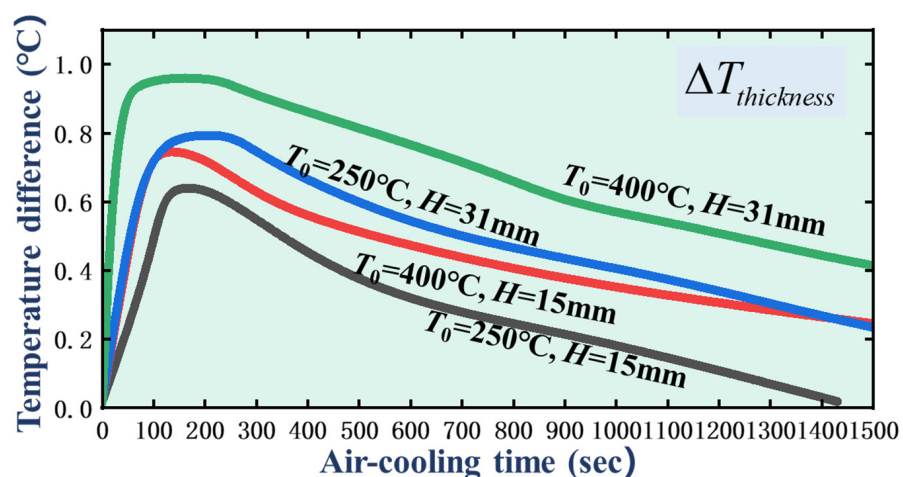


Figure 3. Variation in $\Delta T_{thickness}$ over time under different plate thicknesses and initial temperatures.

The edge and surface layer are uniformly called the 'outer end' and the thickness direction- and width-direction central layers are collectively called the 'central part'. Through the above analysis of heat-dissipation characteristics, it was found that magnesium alloy slabs showed four stages in both width and thickness directions during the air-cooling process (see Figure 4):

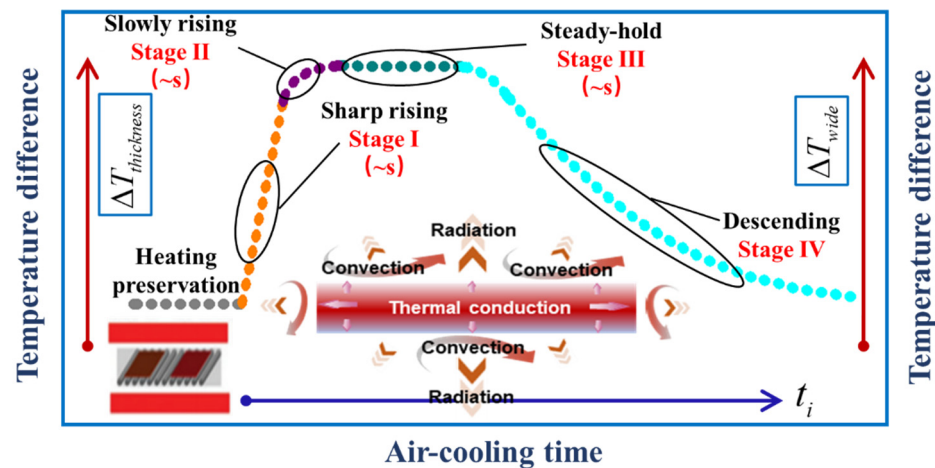


Figure 4. Four stages of temperature-drop curve of magnesium alloy slab during air cooling.

- (1) The process from the beginning of air cooling to the beginning of the central layer temperature reduction, in which there was a sharp increase in the temperature difference between the end face and the central region.
- (2) The temperature of the central part started to decrease. Nevertheless, as the central part conducted heat to the adjacent metal less effectively than the heat dissipation of the end face, the temperature difference between the end face and the central part gradually increased during this process, albeit less sharply than previously.
- (3) The end-face heat dissipation was approximately equal to the heat conduction from the central part to the adjacent metal, in which the maximum temperature difference between the end face and the center part was reached and remained essentially unchanged.
- (4) The heat dissipation of the end face was less than the heat conduction from the center to the adjacent metal and the temperature difference between the end face and the center part decreased gradually.

4. Mathematical Modeling of Air-Cooling Temperature Field

Drawing on the principles of heat transfer, this paper focuses on the phenomenological characteristics of the four aforementioned stages of temperature drop and presents quantitative analysis and modeling of the temperature distribution and evolution of magnesium alloy plates during air cooling. Considering that the plate length is far greater than the width and thickness in the actual rolling production, the heat-dissipation effect of the head-end face and the tail end to the external environment is ignored to simplify the analysis of the heat-transfer process [12]. The method of “discrete dimensionality reduction solution and two-way temperature drop integration” is adopted. First, the entire air-cooling process of the plate can be described as two distinct one-dimensional thermal conduction processes in the width and thickness directions and has symmetry with respect to the central surface. Next, the temperature-drop-calculation results of the same node on the plate in the thickness direction and width direction are superposed to calculate the temperature state of the node affected by air cooling and, therefore, determine the three-dimensional temperature field of the plate in the air-cooling state.

Using the differential element analysis method, the plate was partitioned into layers of elements along both the thickness and the width directions [13,14]. It is assumed that the internal energy of each unit layer increases linearly from the surface layer to the central layer at t_i time. During air-cooling Δt time, the heat-loss degree between layers is also approximately regarded as a linearly decreasing distribution. Taking the thickness direction as an example, the temperature-drop modeling process based on the differential element method is described in detail. Firstly, it can be assumed that the temperature distribution was homogenous at the onset of the process. With the passage of time during the air-cooling process, the cooling effect progressively penetrated into the central layer and the depth of

the temperature drop layer (l_i) gradually expanded. This process included stages I and II, as shown in Figure 5. According to these assumptions, the temperature distribution trend of the temperature-drop layer in the thickness direction can be approximated by a quadratic curve. Until the end of the air-cooling time, t_n , the temperature within the thickness range started to show a complete parabolic curve. This moment was defined as the transition point between stages II and III. Subsequently, the temperature in the thickness direction continued to cool down persistently through heat dissipation following the parabolic curve shape, until entering stage IV of the air-cooling process. At this stage, the temperature of the surface and the center gradually became the same.

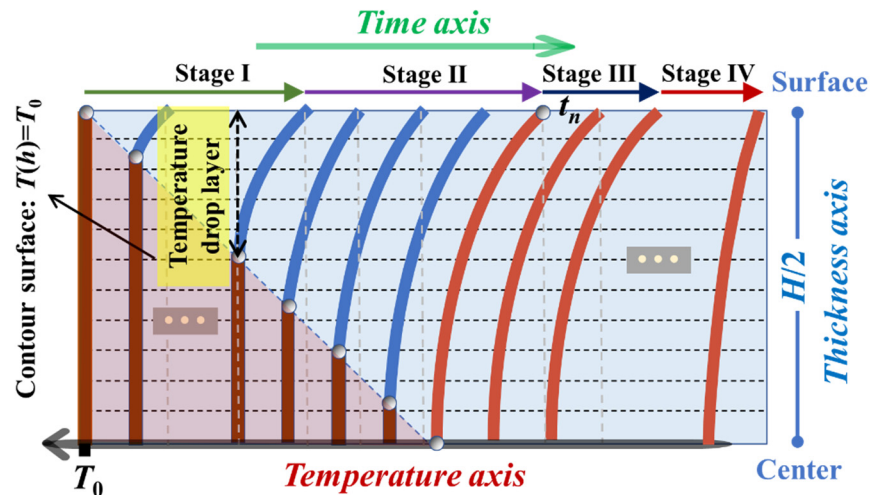


Figure 5. Temperature-distribution trends along the thickness direction of the magnesium plate at different air-cooling stages.

The initial temperature of the plate is T_0 . Before the transition point $t_i \in [t_0, t_n]$ the temperature distribution in the thickness direction of the plate is as follows:

$$T(h) = \begin{cases} T_0 - \frac{T_0 - T_{si}}{l_i^2} (h - l_i)^2 & h \leq l_i \\ T_0 & a_i < h < H - l_i \\ T_0 - \frac{T_0 - T_{si}}{l_i^2} (h - H + l_i)^2 & H - l_i \leq h \leq H \end{cases} \quad (3)$$

where T_0 is discharging temperature of plate; T_{si} is surface temperature of magnesium plate after air cooling for t_i time, $i = 1, 2, 3, n$; l_i is the thickness of temperature-drop zone from the surface after air cooling t_i time; H is thickness of magnesium plate.

Because of the thickness symmetry, the height is taken for modeling research: $h \in [0, H/2]$. According to Fourier’s law, the heat-flow density in the normal direction of the isothermal surface is proportional to the temperature gradient [15] is as follows:

$$\vec{q} = -\lambda \text{grad}(T) \quad (4)$$

$$\text{grad}(T) = \vec{n} \cdot \frac{\partial T}{\partial n} \quad (5)$$

where q is heat flux vector, W/m^2 ; λ is coefficient of thermal conductivity, $W/(m \cdot K)$; $\text{grad}(T)$ is temperature gradient, K/m ; \vec{n} is unit vector of normal direction of isothermal surface.

For one-dimensional steady thermal conduction, according to Fourier’s law, heat-flux density of different sections [16] is as follows:

$$q_i = -2\lambda \cdot \frac{(T_h - T_{si})}{l_i^2} (h - l_i) \quad h \in [0, l_i] \quad (6)$$

Surface, namely $h = 0$, heat flux at t_i is

$$q_i = 2\lambda \cdot \frac{(T_0 - T_{si})}{l_i} \quad (7)$$

Average temperature in thickness direction at t_i is

$$\bar{T}_{ii} = T_0 - \frac{2l_i}{3H} (T_0 - T_{si}) \quad (8)$$

It can be seen from the equations above that the thickness of surface temperature-drop layer at t_i is

$$l_i = \frac{3H}{2} \cdot \frac{T_0 - \bar{T}_{ii}}{T_0 - T_{si}} \quad (9)$$

During air cooling, the plate dissipates heat primarily through thermal radiation and thermal convection. The heat-flow density of the plate surface can be obtained from the Stephen Boltzmann law and Newton's cooling law [17]:

$$\begin{aligned} q_i &= \varepsilon\sigma(T_{si}^4 - T_{Air}^4) + \gamma(T_{si} - T_{Air}) \\ &= \eta(T_{si} - T_{Air}) \end{aligned} \quad (10)$$

where ε is the emissivity of magnesium alloy plate, which is equal to the ratio of the emissivity of the actual object to the emissivity of the blackbody at the same temperature, which is a constant between 0 and 1; σ is blackbody radiation constant, whose value is equal to $5.67 \text{ W}/(\text{m}^2 \cdot \text{K}^4)$ [18]; γ is convective-heat-transfer coefficient between plate metal and air, whose value is $30 \text{ W}/(\text{m}^2 \cdot \text{K})$ [19]; T_{Air} is air temperature; η represents the comprehensive heat-transfer coefficient when in contact with air and is equal to $\eta = \varepsilon\sigma(T_{si} + T_{Air})(T_{si}^2 + T_{Air}^2) + \gamma$.

According to (6), (7) and (8), at t_i ,

$$\bar{T}_{ii} = T_0 - \frac{4\lambda(T_0 - T_{si})^2}{3H\eta(T_{si} - T_{Air})} \quad (11)$$

In a short time, the heat flux per unit area can be considered as a fixed value. According to the law of energy conservation, the heat loss from heat exchange with air is equal to the reduction in internal energy of plate metal [20]:

$$c\rho \frac{H}{2} \cdot \frac{2l_i}{3H} (T_0 - T_{si}) = \int_0^{\Delta t_i} q_i dt \quad (12)$$

Bringing Equation (7) into Equation (12), we can obtain

$$\int_0^{\Delta t_i} q_i dt = 2\lambda \cdot \frac{(T_0 - T_{si})}{l_i} \Delta t_i \quad (13)$$

$$l_i = \sqrt{\frac{6\lambda\Delta t_i}{\rho c}} \quad (14)$$

where c is specific heat capacity of plate and ρ is plate density.

Next, we divide the cooling time into small portions. At the initial time, the thickness of the temperature-drop layer can be obtained according to Δt_i and Equation (14). Because the time is sufficiently short, the surface-heat-flow density can be calculated according to Equation (10), after which $T_0 - T_{si}$ can be calculated according to Equation (7), that is, the temperature drop on the surface of the plate within Δt_i time. Combined with the initial temperature, the surface temperature of the plate T_{si} at Δt_i time can be calculated. According to the surface temperature and the thickness of the temperature-drop layer a_i at Δt_i time, the thickness-direction temperature field of the first stage ($t_i \in [t_0, t_n]$) can be

solved through Equation (3). Next, the average thickness-direction temperature at any time can be determined according to Equation (11).

As the temperature continues to decrease, the temperature distribution from the surface layer to the center begins to exhibit a complete parabolic shape within the specified time range of $t_i \in [t_n, \infty]$. The trend of temperature distribution along the thickness direction of plate metal meets the following requirements:

$$T(h) = T_{ci} - \frac{4(T_{ci} - T_{si})}{H^2} \left(h - \frac{H}{2}\right)^2 \quad 0 \leq h \leq H \quad (15)$$

Average temperature in thickness direction at this time:

$$\bar{T}_{ti} = \frac{T_{si} + 2T_{ci}}{3} \quad (16)$$

At this time, the surface heat flux is determined by Equation (6). Let $a_i = H/2$:

$$q_i = 4\lambda \cdot \frac{(T_{ci} - T_{si})}{H} \quad (17)$$

Similarly, the heat-flow density q_i at this time is calculated according to Equation (10) through T_{si} . Furthermore, combining Equations (16) and (17), we can obtain

$$T_{si} = \bar{T}_{ti} + \frac{Hq_i}{6\lambda} \quad (18)$$

After several iterations, the temperature distribution along the thickness direction in the subsequent stage can be determined.

Based on the model described above, the temperature distribution of the magnesium plate is calculated separately for the thickness and width directions. Finally, the temperature drop in the two directions at the same cooling time is superposed to calculate the temperature of each point. The temperature-distribution model along the width direction at a particular thickness h_y ($0 \leq h_y \leq H$) is:

$$T_h(w) = T_0 - \Delta T_{\text{thickness}}(h) - \Delta T_{\text{wide}}(w) \quad (19)$$

where $T_h(w)$ is the temperature at [thickness direction position, width direction position] = [h, w] after air cooling t_i time; $\Delta T_{\text{thickness}}(h)$ is the temperature drop calculated by the thickness-direction model; $\Delta T_{\text{wide}}(w)$ is the temperature drop calculated by the width direction model.

Thermal-physical parameters (including specific heat capacity c and thermal conductivity λ) are calculated by the simulation software for materials' properties, JMatPro, as functions of temperature when taking all phases into account. The least squares fitting function in MATLAB software is used to perform nonlinear fitting on the relevant functional relationship. Figure 6 shows the comparison between the fitting curves and the experimental calculated values.

According to $\eta = \varepsilon\sigma(T_{si} + T_{\text{Air}})(T_{si}^2 + T_{\text{Air}}^2) + \gamma$, it is necessary to obtain the accurate values of ε and γ to determine the value of the comprehensive heat-transfer coefficient during air cooling of magnesium alloy plate [21,22]. Due to the influence of complex material and environmental factors (e.g., surface geometric state, thermal state, air velocity, material physical properties, etc.), it is difficult to directly measure these two variables (ε and γ) and their changing trend with time by physical experimental method. Therefore, we used a combination of finite element simulation and physical experiment to obtain η . The results are shown in Figure 7.

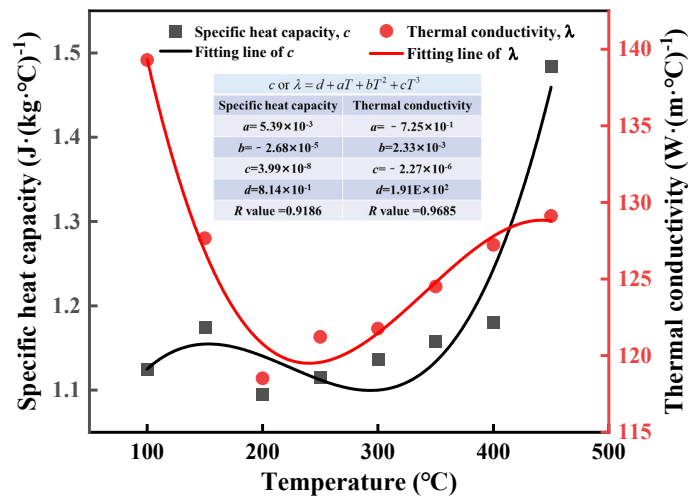


Figure 6. Specific heat capacity and thermal conductivity of AZ31B alloy under different temperatures.

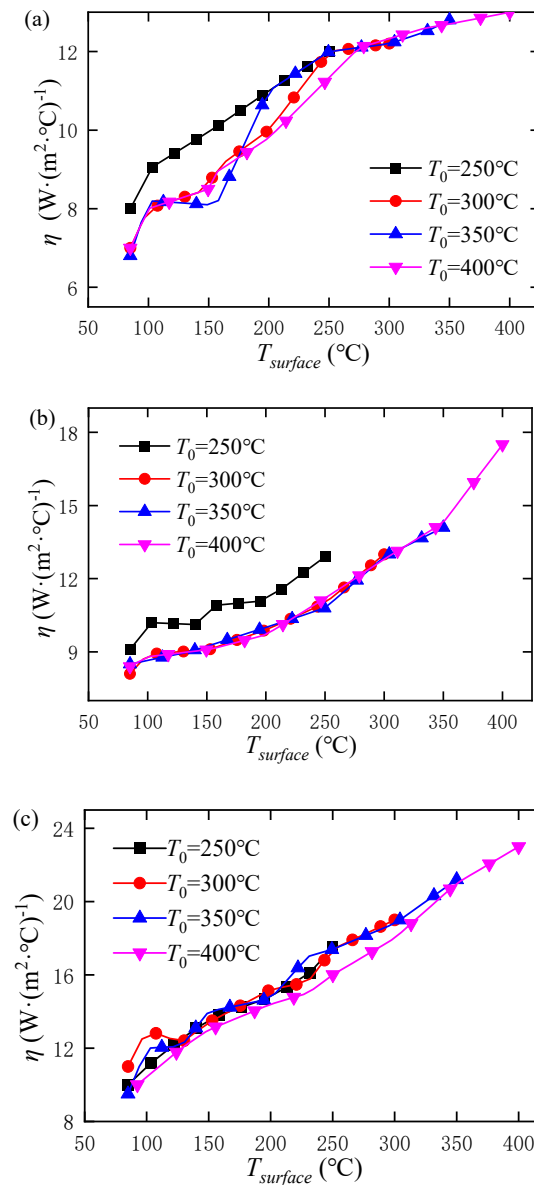


Figure 7. Variation in η over initial temperature and cooling time η under different thicknesses. (a) 8 mm; (b) 15 mm; (c) 31 mm.

Based on the analysis of phenomenological characteristics of heat-transfer-coefficient curves in Figure 7, the nonlinear least squares fitting method is utilized to derive the expression of η : $\eta(T_{surface}, H) = 0.4361 \cdot H^{0.7} \cdot T_{surface} + 6.947$. It is verified that the formula has high accuracy in fitting the comprehensive heat-transfer coefficient under experimental conditions, the relative error under different conditions is less than 10% and the correlation coefficient (R) is 0.9882.

5. Applicability Evaluation of Temperature Model

According to Figures 2 and 3, the temperature distribution in thickness direction was more uniform than that in the width direction. The maximum temperature difference in the width direction of the experimental specification plate reached 10 °C, while the temperature difference in the thickness direction was only about 1 °C. Therefore, the model's applicability evaluation was only conducted for different positions along the width direction of the plate surface. The relation between the predicted and experimental curves of the ΔT_{width} variation over time at 400 °C–15 mm and 250 °C–15 mm is shown in Figure 8. It can be observed that the model's predictions for the temperature difference were relatively close to the actual experimental results and accurately depicted the single-peak characteristics. However, the predicted peak value was higher than the actual value and the timing of the peak occurrence lagged behind the actual value. This may have been due to the model's inadequate expression of self-conduction in the width direction or an excessive representation of heat radiation and convective heat transfer. Taking the experimental conditions of a plate thickness of 31 mm and initial temperatures of 400 °C and 250 °C as examples, Figure 9 displays a comparison between the predicted temperature and the experimental temperature over time at different positions in the width direction. It can be seen that the predicted results of the model were relatively close to the experimental results when the air-cooling time was within 0~150 s. With the continuation of the heat-dissipation process, the prediction deviation of the model increased. However, the deviation was no more than 15 °C when the air-cooling time was within 0~500 s, which indicates that the temperature model based on the characteristics of the four stages of heat dissipation and cooling had a wider application range.

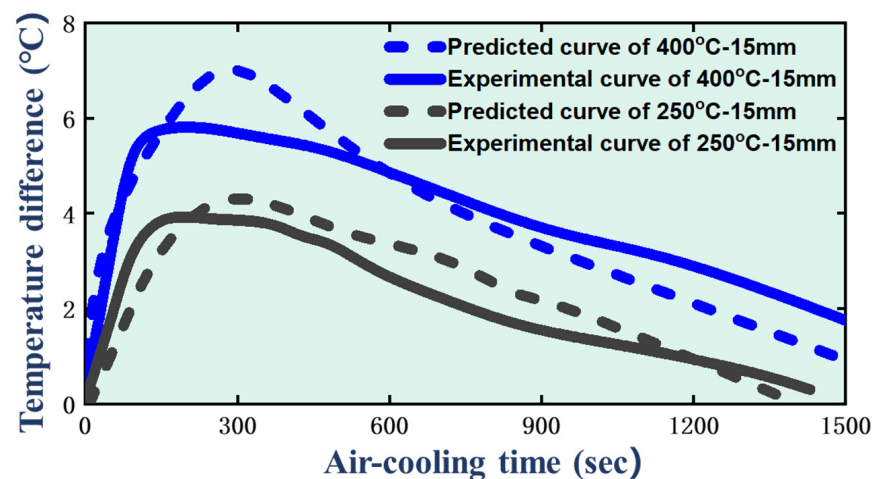


Figure 8. Relation between the predicted and experimental curves of ΔT_{width} variation at 400 °C–15 mm and 250 °C–15 mm.

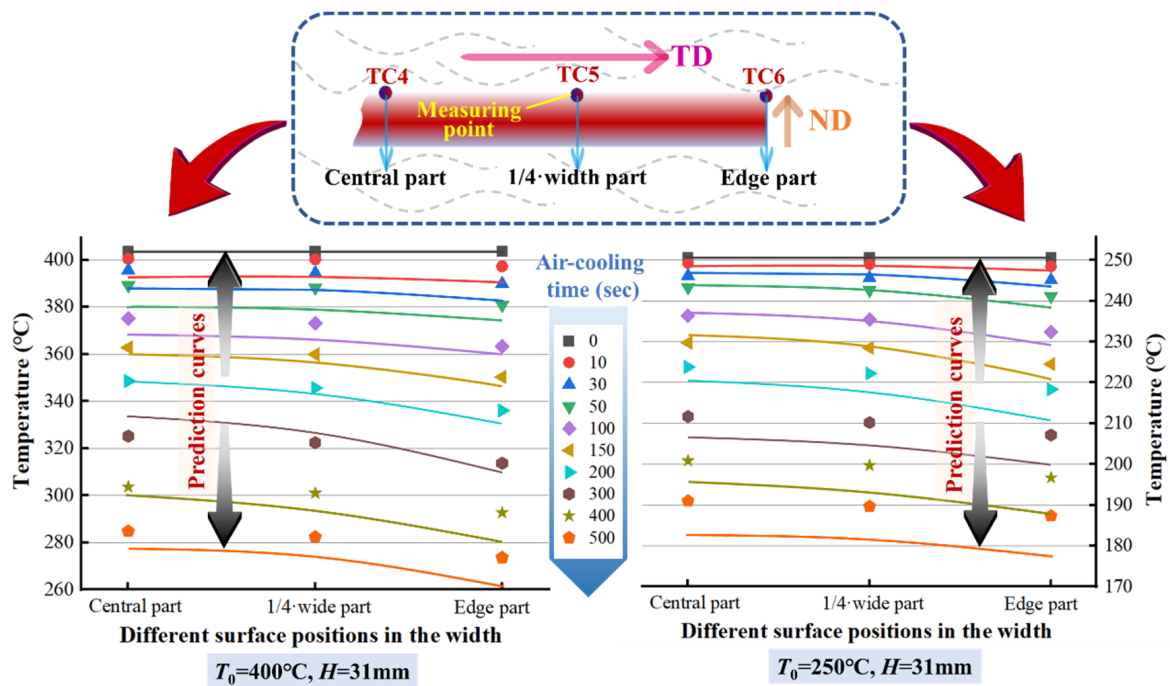


Figure 9. Comparison between calculated and experimental temperatures at different width positions during the air-cooling process under 400°C – 31 mm and 250°C – 31 mm .

6. Conclusions

In the air-cooling process of the magnesium alloy plates, temperature non-uniformity was observed in both the thickness and width directions, with the latter being more severe. The degree of non-uniformity strongly depended on the initial temperature and plate thickness. The temperature difference between the end and center of the plate exhibited a single-peak feature over time, occurring during the 140–200-s period after the air-cooling began. During the roller-conveying process, it is recommended to heat the plate before this period to facilitate efficient reheating and ensure the subsequent rolling temperature.

By separately calculating one-dimensional heat-transfer models in the width and thickness directions and then integrating them reasonably to account for bi-directional cooling, it is possible to accurately describe the heat dissipation and cooling laws of magnesium-alloy-plate air-cooling. The deviation in the predicted temperature within the 0–500-s cooling-time range was no more than 15°C . The inadequate expression of self-conduction in the width direction or an excessive representation of heat radiation and convective heat transfer constitute the primary sources of error in the modeling process. In reality, the evolution of temperature is more complex and the interaction of various heat-transfer mechanisms still needs to be accurately quantified.

Author Contributions: Methodology, X.C. and S.X.; Validation, Z.W.; Formal analysis, Z.W. and Y.D.; Investigation, S.X.; Data curation, Z.W. and W.J.; Writing—original draft, Z.W.; Supervision, S.X.; Project administration, W.J. and X.C.; Funding acquisition, S.X. and W.J. All authors have read and agreed to the published version of the manuscript.

Funding: This work is supported by the National Natural Science Foundation of China (nos. 62102280 and 52105388), Fundamental Research Program of Shanxi Province (no. 20210302124167) and Key Research and Development Program of Shanxi Province (nos. 202102020101001, 202102050201005 and 202102020101007).

Conflicts of Interest: The authors declare no conflict of interest.

References

1. Nam, A.; Prufert, U.; Pietrzyk, M.; Kawalla, R.; Prah, U. Simulation of Thermal Phenomena in Reverse Strip-Rolling Process. *Mater. Sci. Forum* **2018**, *941*, 1424–1430. [[CrossRef](#)]
2. Chen, D.; Zhang, R.; Li, Z.; Li, Y.; Yuan, G. Temperature distribution prediction in control cooling process with recurrent neural network for variable-velocity hot rolling strips. *Int. J. Adv. Manuf. Technol.* **2022**, *120*, 7533–7546. [[CrossRef](#)]
3. Jang, J.-Y.; Guo, J.-W.; Chang, C.-C. The Heat Transfer Analysis of an Acting-type Heat Retention Panel used in a Hot Rolling Process. *Appl. Sci.* **2019**, *9*, 189. [[CrossRef](#)]
4. Nikitenko, N.I. Temperature field calculation from body deformation measurements. *J. Eng. Phys.* **1980**, *3*, 877–880. [[CrossRef](#)]
5. Jia, W.; Tang, Y.; Le, Q.; Cui, J. Air-cooling analysis of AZ31B magnesium alloy plate: Experimental verification, numerical simulation and mathematical modeling. *J. Alloy Compd.* **2017**, *2*, 1838–1853. [[CrossRef](#)]
6. Le, Q.; Jia, W.; Ning, F. Heat transfer analysis of magnesium alloy plate during transport process. *J. Magnes. Alloy* **2019**, *7*, 291–296. [[CrossRef](#)]
7. Fic, A.; Nowak, A.J.; Bialecki, R. Heat transfer analysis of the continuous casting process by the front tracking BEM. *Eng. Anal. Bound. Elem.* **2000**, *3*, 215–223. [[CrossRef](#)]
8. Xu, Z. Mathematical Model for Temperature Control in Hot Strip Finishing Mill Group. *Mater. Sci.* **2003**, *15*, 19–23.
9. Bettles, C.; Barnett, M. *Advances in Wrought Magnesium Alloys*; Woodhead: Cambridge, UK, 2012; p. 350.
10. Feng, J.C.; Wang, Y.R.; Zhang, Z.D. Nugget growth characteristic for AZ31B magnesium alloy during resistance spot welding. *Sci. Technol. Weld. Join.* **2006**, *11*, 154–162. [[CrossRef](#)]
11. Chang, Z.; Li, M.; Zhu, K.; Sun, L. Model predictive control of long Transfer-line cooling process based on Back-Propagation neural network. *Appl. Therm. Eng.* **2022**, *5*, 1359–4311. [[CrossRef](#)]
12. Chen, D.; Zhang, R.; Li, Y.; Li, Z.; Guo, Y. *Online Cooling System and Improved Similar Self-Adaptive Strategy for Hot-Rolled Seamless Steel Tube*; ISIJ International: Tokyo, Japan, 2021; p. 6.
13. Zhao, Y.; Yang, W.; Hou, H. A New Kind of FDM/FEM Squeeze Casting Temperature Field Calculation Model. *Adv. Mater. Res.* **2013**, *3*, 641–642. [[CrossRef](#)]
14. Wan, H.; Zhao, L. Temperature Field Calculation of Mass Concrete Anchor. *Appl. Mech. Mater.* **2012**, *5*, 166–169. [[CrossRef](#)]
15. Wang, X. Effects of constitutive parameters on adiabatic shear localization for ductile metal based on JOHNSON-COOK and gradient plasticity models. *Trans. Nonferrous Met. Soc. China* **2006**, *9*, 1362–1369. [[CrossRef](#)]
16. Storchak, M.; Kushner, V.; Möhring, H.-C.; Thomas, S. Refinement of temperature determination in cutting zones. *J. Mech. Sci. Technol.* **2021**, *7*, 3659–3673. [[CrossRef](#)]
17. Dittrich, W.; Minkin, L. Measuring the Specific Heat of Metals by Cooling. *Phys. Teach.* **2010**, *10*, 531–533. [[CrossRef](#)]
18. Giovanni, T.; Mario, M. Effects of Surface Irregularities and Coatings on Thermal Emittance of Selected Metals Between 373 and 1073 K. *J. Heat Transf.* **2021**, *4*, 9.
19. Kurtulus, E.; Sapmaz, I.; Karpat, F. Effect of the cooling process on the mechanical properties and microstructural behavior of extruded AZ31 and AM50 Mg alloys. *Mater. Test.* **2021**, *63*, 654–661. [[CrossRef](#)]
20. Peleshenko, B.I.; Kravchenko, Y.G.; Burya, A.I.; Kovalenko, A.V. Temperature Field Calculation on the Counterbody Strip Tribosurface. *J. Frict. Wear* **2012**, *8*, 239–243. [[CrossRef](#)]
21. Zhang, Y.; Shen, H.; Zhu, R. Temperature Field Calculation of Anisotropic Crystal in the Photothermal Displacement Detection Theory. *Adv. Mater. Res.* **2013**, *7*, 718–720. [[CrossRef](#)]
22. Serikov, A.V.; Kuz'min, V.M. A three-dimensional temperature field calculation for a transformer-type heating element. *Russ. Electr. Eng.* **2012**, *7*, 209–214. [[CrossRef](#)]

Disclaimer/Publisher's Note: The statements, opinions and data contained in all publications are solely those of the individual author(s) and contributor(s) and not of MDPI and/or the editor(s). MDPI and/or the editor(s) disclaim responsibility for any injury to people or property resulting from any ideas, methods, instructions or products referred to in the content.